NANO LETTERS

pubs.acs.org/NanoLett Letter

Anomalous Second Harmonic Generation from Atomically Thin $MnBi_2Te_4$

Jordan Fonseca, Geoffrey M. Diederich, Dmitry Ovchinnikov, Jiaqi Cai, Chong Wang, Jiaqiang Yan, Di Xiao, and Xiaodong Xu*

Cite This: *Nano Lett.* 2022, 22, 10134−10139 Read Online

ACCESS | Metrics & More | Article Recommendations | Supporting Information

ABSTRACT: $MnBi_2Te_4$ is a van der Waals topological insulator with intrinsic intralayer ferromagnetic exchange and A-type antiferromagnetic interlayer coupling. Theoretically, it belongs to a class of structurally centrosymmetric crystals whose layered antiferromagnetic order breaks inversion symmetry for even layer numbers, making optical second harmonic generation (SHG) an ideal probe of the coupling between the crystal and magnetic structures. Here, we perform magnetic field and temperature-dependent SHG measurements on $MnBi_2Te_4$ flakes ranging from bulk to monolayer thickness. We find that the dominant SHG signal from $MnBi_2Te_4$ is unexpectedly unrelated to both magnetic state and layer number. We suggest that surface SHG is the likely source of the observed strong SHG, whose symmetry matches that of the $MnBi_2Te_4$−vacuum interface. Our results highlight the importance of considering the surface contribution to inversion symmetry-breaking in van der Waals centrosymmetric magnets.

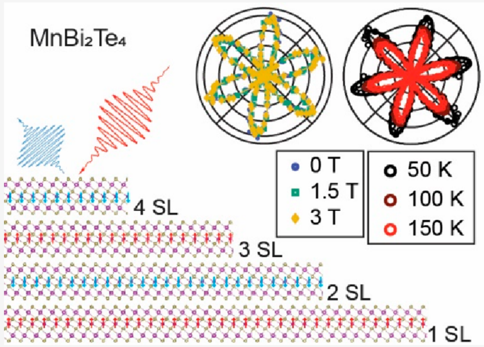

KEYWORDS: *topological magnets, second harmonic generation, surface symmetry-breaking, centrosymmetric magnets, 2D magnets*

$MnBi_2Te_4$ has attracted broad interest in recent years due to its potential to host intertwined intrinsic magnetic and topological properties that persist to the atomically thin limit.[1−7] It is a van der Waals crystal in which each stoichiometric septuple layer (SL) can be thought of as a quintuple layer of Bi_2Te_3 intercalated with an MnTe bilayer (Figure 1a).[8,9] The Mn spins in each SL couple ferromagnetically to each other with magnetic moments along the easy *c*-axis; however, exchange coupling causes spins in adjacent layers to antialign, giving rise to A-type antiferromagnetic (AFM) ordering below the Néel temperature of $T_N \approx 25$ K.[1,7] The interplay of thickness, magnetic state, and band topology conspire to produce a rich topological phase diagram. $MnBi_2Te_4$ is predicted to host a trivial magnetic insulator in 1 SL flakes, the zero-plateau quantum anomalous Hall effect or "axion insulator states" in thin even-layer flakes, and quantum anomalous Hall (QAH) states in thin odd-layer flakes.[10]

Despite the excitement precipitated by this theoretical work, robust and consistent experimental evidence for $MnBi_2Te_4$'s thickness-dependent physics has remained elusive. Shortly after the initial theoretical prediction,[10] the material was synthesized in bulk crystal form and confirmed to be the first AFM topological insulator.[8,9] Subsequent experimental works on atomically thin flakes partially confirmed initial predictions, with the observation of the QAH effect in a 5 SL device[6] and transport signatures of the axion insulator state in 6 SL samples.[11] Nevertheless, reproducing the QAH effect has been difficult. Instead, quantized transport in the field induced ferromagnetic state has been repeatedly observed and become a robust phenomenon in both even- and odd-layer samples. Thus, the nature of $MnBi_2Te_4$'s layer-dependent topological and magnetic states remains an open question.

Besides numerous transport studies indicating similar magnetic-state-dependent topological properties of even- and odd-layer number samples,[3,11−17] Angle-resolved photoemission spectroscopy measurements provide inconclusive results regarding whether the surface state is gapped at zero magnetic field.[18−20] These experimental incongruities might be related to the impact of atomic defects on magnetism,[21] defect-induced surface reconstruction in few-layer samples,[22] or a possible exfoliation-induced structural or magnetic phase transition,[23−25] all of which could alter the expected layer-dependent magnetism and topology of the studied samples. This situation calls for a noninvasive probe that is sensitive to $MnBi_2Te_4$'s layer-dependent structural, magnetic, and surface symmetries.

Optical second harmonic generation (SHG) is an ideal tool to investigate $MnBi_2Te_4$'s structural and magnetic properties. Within the 2D materials field, SHG arising from structural

Received: October 12, 2022
Revised: December 1, 2022
Published: December 7, 2022

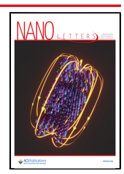

https://doi.org/10.1021/acs.nanolett.2c04010
Nano Lett. 2022, 22, 10134−10139

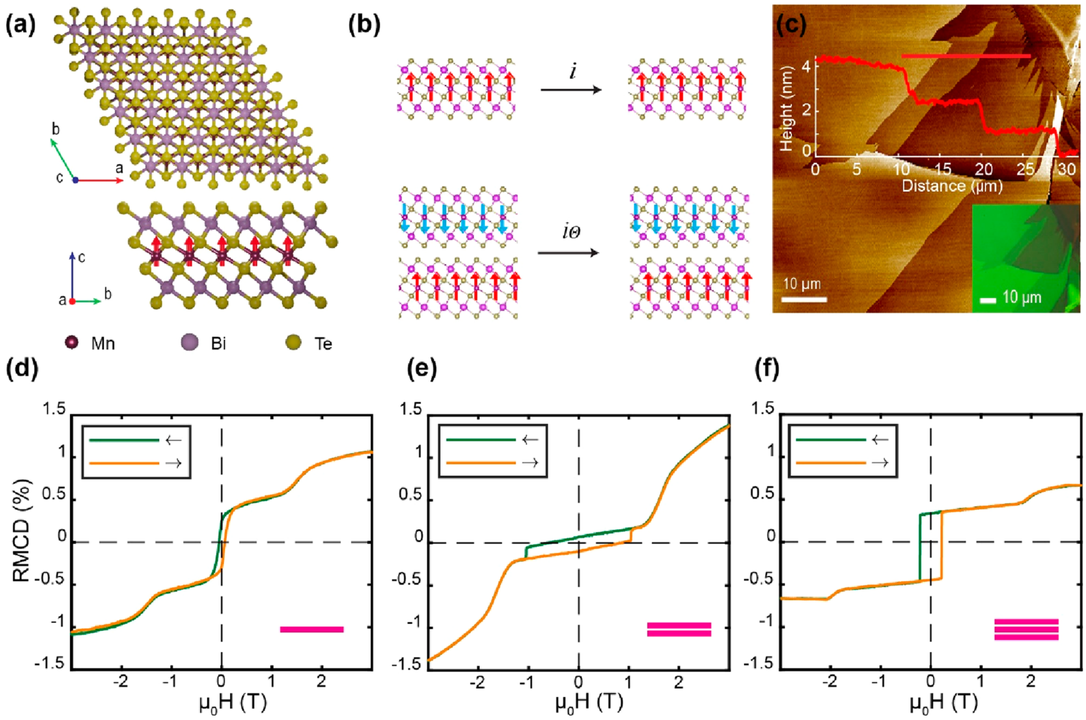

Figure 1. $MnBi_2Te_4$ crystal structure and magnetic ordering. (a) $MnBi_2Te_4$ crystal structure. (b) Schematic showing how symmetry is preserved (broken) in odd (even) layer crystals. Red/blue arrows indicate the magnetic ground state below the Néel temperature. (c) Atomic force microscope image of $MnBi_2Te_4$ flakes down to a monolayer with linecut of 1 SL, 2 SL, and 3 SL steps taken along red line. Inset shows optical image of the same region. (d−f) Reflectance magnetic circular dichroism sweeps of 1 SL, 2 SL, and 3 SL flakes measured at ∼4.5 K. Magenta insets indicate $MnBi_2Te_4$ layer number measured in each plot.

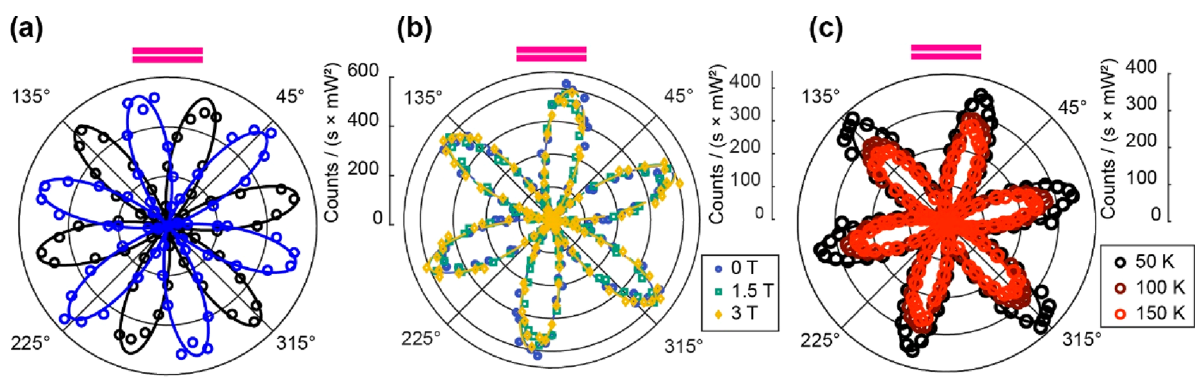

Figure 2. 2 SL $MnBi_2Te_4$ magnetic field and temperature-dependent SHG. (a) Polarization-resolved SHG from 2 SL $MnBi_2Te_4$ with no applied field below the Néel temperature. Black (blue) dots are co(cross)-linearly polarized experimental data with solid line fits to eq 1 (eq 2) (Supporting Information). XY data are excluded from subsequent subfigures for clarity. (b) Out-of-plane magnetic field dependence of the SHG. (c) Temperature dependence of the SHG above T_N. Magenta insets indicate $MnBi_2Te_4$ layer number measured in each plot. All data in (b) and (c) are taken at a cryostat base temperature of ∼4.5 K, and only XX data are shown for clarity.

inversion symmetry-breaking has found utility as a noninvasive means to optically identify crystal axes,[26,27] measure strain,[28] and identify relative twist-angle in layered materials.[29−32] Furthermore, inversion symmetry can be broken by an A-type AFM order (Figure 1b), leading to so-called c-type SHG. It has been employed to explore structural and magnetic properties of a variety of materials including bulk Cr_2O_3,[33] atomically thin $MnPS_3$,[34] bilayer CrI_3,[35] and monolayer $MnPSe_3$.[36] Studies have shown that $MnBi_2Te_4$ crystallizes in the centrosymmetric $R\bar{3}m$ (D_{3d}^5) space group.[37−39] With A-type AFM magnetic ordering included, this becomes the magnetic space group $R_I\bar{3}c$[40] with the crystal and magnetic structure depicted in Figure 1a,b. In even (odd) layers, strong (zero) c-type SHG is predicted,[41] making optical second harmonic generation a feasible probe of both AFM order and the symmetries of the underlying crystal structure with particular sensitivity to the surface.

In this work, we perform polarization-resolved SHG and polar reflectance magnetic circular dichroism (RMCD) measurements on $MnBi_2Te_4$ flakes ranging in thickness from bulk to monolayer. Contrary to our expectations, we find that the observed SHG is independent of magnetic state, temperature, exfoliation substrate, or crystal thickness. We conclude that any c-type SHG arising from the AFM ordering is obscured by a much stronger signal that likely arises from the interface between $MnBi_2Te_4$ and vacuum. Our findings are

https://doi.org/10.1021/acs.nanolett.2c04010
Nano Lett. 2022, 22, 10134−10139

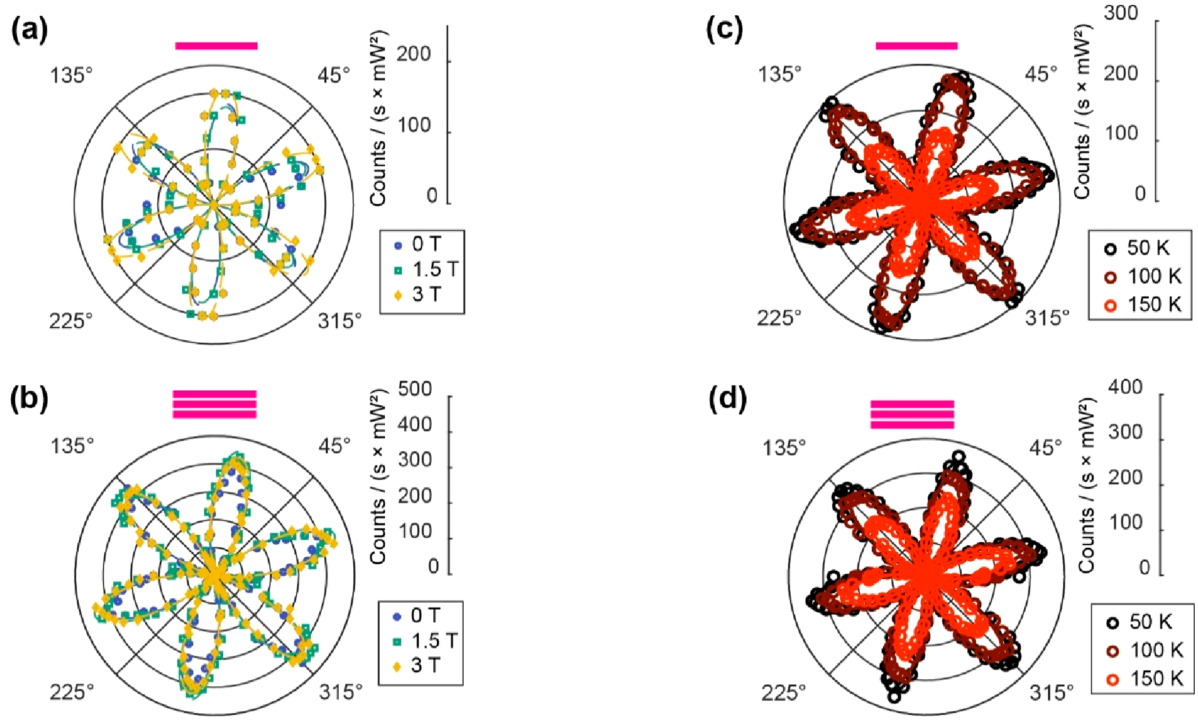

Figure 3. 1 SL and 3 SL magneto- and temperature-dependent SHG. Dependence of the XX SHG on an out-of-plane magnetic field for 1 SL (a) and 3 SL flakes (b) at a base temperature of ~4.5 K. Temperature dependence of the XX SHG for 1 SL (c) and 3 SL (d) flakes above T_N. Magenta insets indicate $MnBi_2Te_4$ layer number. XY data, which exhibit the same behavior, are omitted for clarity.

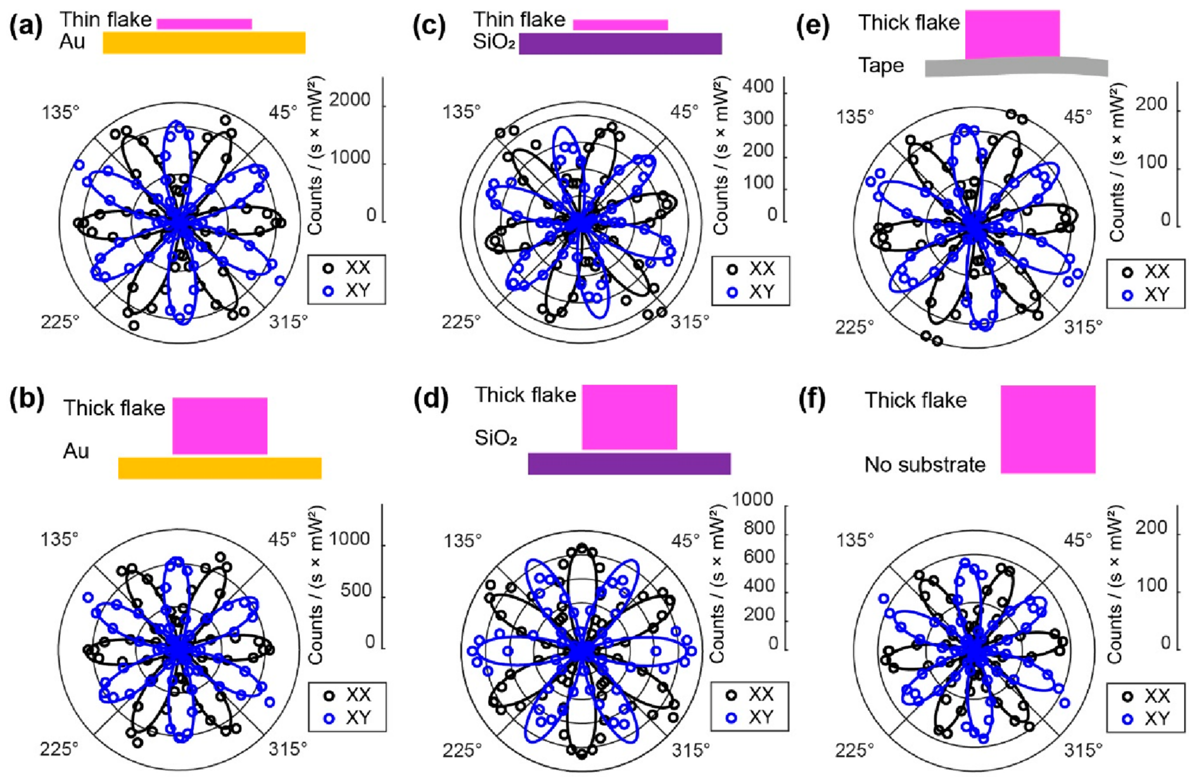

Figure 4. Thickness and substrate dependence of polarization-resolved SHG. Polarization-resolved SHG from a (a) few-layer flake on Au, (b) bulk flake on Au, (c) few-layer flake on SiO_2, (d) bulk flake on SiO_2, (e) bulk flake cleaved on Scotch tape before exfoliation, and (f) pristine bulk flake oriented to have the beam incident on the (0001) surface. All data are taken at cryogenic temperature with no applied magnetic field. Black (blue) dots are co(cross)-linearly polarized experimental data with solid line fits to eq 1 (eq 2) in the Supporting Information.

consistent with the expected structural symmetry of $MnBi_2Te_4$ and call for additional studies to address the underlying reasons for the absence of observation of c-type SHG.

After preparing 1−4 SL flakes of $MnBi_2Te_4$ (Figure 1c, Methods in the Supporting Information), we characterize the layer-dependent magnetic state using RMCD, which is a sensitive optical probe of out-of-plane magnetization for 2D materials.[42] We demonstrate that our layer assignment, magnetization curves, spin-flip coercive fields, and spin-flop/spin-canting fields are consistent with existing literature (Figure 1d−f and Figure S1a).[4,7] We then employ polarization-resolved SHG measurements on the same 1−4 SL flakes characterized with RMCD to compare their magnetic state with their SHG response. We measure the colinear (XX) and cross-linear (XY) SHG response in Faraday geometry, which enables us to maximally probe the elements of the nonlinear susceptibility tensor given the normal incidence restrictions of our measurement apparatus.

At first glance, the SHG response from 2 SL $MnBi_2Te_4$ is consistent with the theoretical prediction (Figure 2a). A six-fold pattern emerges in both XX and XY channels, which have identical amplitudes and can be fit well by the predicted theoretical model based on AFM time reversal symmetry-breaking (Methods in the Supporting Information).[41] Unexpectedly, the observed pattern remains unchanged under applied magnetic field up to 3 T (Figure 2b), which is above the 2 SL spin flop field of ∼2 T.[4,7] For an SHG signal arising from AFM ordering that breaks inversion symmetry, we expect a change in the underlying magnetic state to manifest as a change to the shape or amplitude of the SHG rotational anisotropy. Experimentally, we do not see this change, which suggests that time reversal symmetry-breaking is not the mechanism that explains the observed signal. We more conclusively demonstrate the independence of the measured SHG signal on magnetic ordering with temperature-dependent measurements. As shown in Figure 2c, the SHG anisotropy and amplitude from the 2 SL remain nearly unchanged up to 150 K (Figure 2c) which far exceeds the Néel temperature of ∼25 K.

We observe nearly identical behavior in 1 SL and 3 SL samples. Regardless of magnetic state, all odd-layer flakes of $MnBi_2Te_4$ possess an inversion center located at the middle Mn layer, which should make these layers second-harmonic dark. Surprisingly, we find that the SHG from 1 SL and 3 SL flakes is as strong as that from the 2 SL with identical polarization dependence. As with the 2 SL flake, SHG from 1 SL and 3 SL samples exhibits no magnetic field dependence up to 3 T (Figure 3a,b) and remains unchanged at temperatures far above the Néel temperature (Figure 3c,d). Therefore, the observed SHG has no magnetic origin. A 4 SL sample also exhibits nearly identical behavior (Figure S1). The fluctuations in intensity observed in the temperature dependence data do not reflect a real change in the sample, but rather imperfect experimental conditions across the wide temperature range.

To ensure that our fabrication methods have not introduced any unwanted signal contributions, we explore how the SHG from $MnBi_2Te_4$ depends on flake substrate and crystal thickness. For example, charge transfer between the Au substrate and the atomically thin $MnBi_2Te_4$ flakes we measured could result in a symmetry-breaking electric field arising within the crystal.[43] To understand the impact this effect has on our data, we compare the SHG from thin and thick flakes exfoliated onto either Au or SiO_2 (Figure 4a−d). Although there is variation in intensity across the plots shown, no pattern emerged in our measurements that would allow us to identify a consistent trend between flakes exfoliated on gold versus SiO_2. Crucially, choice of substrate does not explain the presence of the SHG signal that we observe. Finally, we rule out an exfoliation-induced structural transition by performing SHG measurements at various stages of our flake preparation. We measure SHG from the (0001) surface of bulk $MnBi_2Te_4$ (Figure 4f) as well as from flakes that have been cleaved onto scotch tape but not deposited onto any substrate (Figure 4e). We find that the SHG from unexfoliated bulk flakes is typically ∼5 times weaker than that measured from exfoliated bulk flakes, but that otherwise the shape and presence of $MnBi_2Te_4$'s rotational anisotropy SHG response is independent of crystal thickness, exfoliation substrate, and exfoliation process. At 800 nm, the nonlinear susceptibility of exfoliated bulk $MnBi_2Te_4$ is ∼50 times weaker than the susceptibility of monolayer WSe_2 (Figure S2). While the 5-fold change in the SHG intensity across a wide variety of sample thicknesses and preparation methods may be indicative of some symmetry-breaking process that occurs during the exfoliation, it does not explain the presence of SHG in the remainder of our measurements.

Our experimental results conclusively reveal that the dominant second harmonic response of $MnBi_2Te_4$ crystals of all thicknesses under 800 nm excitation is unrelated to the material's magnetic properties. Rather, the system exhibits a layer-, magnetic-state-, and temperature-independent response which cannot arise from the centrosymmetric crystal structure of both bulk and monolayer flakes. We note that our experiment does not preclude the existence of the predicted c-type SHG, which might be much stronger for mid-IR excitation wavelengths.[41] If there is any c-type SHG, any additional contribution this makes to the dominant i-type signal cannot be resolved in our measurements. More specifically, this may be because our excitation energy of ∼1.55 eV (800 nm) is much smaller than the spin splitting between the Mn d-bands[44] that would give rise to a strong c-type SHG signal.

The unexpectedly strong and magnetic-state-independent SHG response of $MnBi_2Te_4$ calls for further investigation into the origin of this signal. SHG in centrosymmetric crystals can arise from magnetic dipole or toroidal moments,[45] though we rule out any magnetic contributions to our signal on the grounds that these contributions would depend on applied magnetic field and temperature, contrary to our observations. For a more plausible explanation of the origin of the anomalous SHG signal, we look to $MnBi_2Te_4$'s parent materials Bi_2X_3 (X = Te, Se), both of which exhibit SHG arising from the inversion symmetry-broken surface of the crystal where the crystallographic point group symmetry is reduced from D_{3d} to C_{3v},[43,46] as is the case for $MnBi_2Te_4$. In Bi_2Se_3, rotational anisotropy and surface oxidation-dependent SHG measurements confirm that the 6-fold SHG pattern originates from the anharmonic hyperpolarizability of the Bi−Se and Se−Se bonds at the surface.[43] SHG from $MnBi_2Te_4$ also exhibits strong dependence on the surface oxidation (Figure S3) as well as a rotational anisotropy consistent with the C_{3v} point group. Both of these facts point toward anharmonic polarizability of the in-plane Te−Te bonds at the crystal surface as the main source of the SHG reported here. Because the point group symmetry at an interface is related to the bulk material's point group, our surface SHG

https://doi.org/10.1021/acs.nanolett.2c04010
Nano Lett. 2022, 22, 10134−10139

measurements corroborate $MnBi_2Te_4$'s expected crystal structure and stacking order.

In conclusion, we use RMCD to characterize the layer-dependent magnetic ordering of few-layer $MnBi_2Te_4$ down to a monolayer. We subsequently employ polarization-resolved magneto- and temperature-dependent SHG to show that, contrary to expectations, the measured SHG pattern at 800 nm excitation is independent of the material's magnetic ordering and layer thickness. We emphasize that our most important finding is that the SHG generated from widely available Ti:sapphire sources does not probe AFM magnetic order in $MnBi_2Te_4$, but rather likely arises from an inevitable structural symmetry-breaking at the crystal surface. Our results lay the experimental groundwork for future nonlinear optical studies of the magnetic and structure properties in topological antiferromagnet $MnBi_2Te_4$.

■ ASSOCIATED CONTENT

Data Availability Statement

The data that support the findings of this study are available from the corresponding authors upon reasonable request.

Supporting Information

The Supporting Information is available free of charge at https://pubs.acs.org/doi/10.1021/acs.nanolett.2c04010.

Experimental methods, 4 SL RMCD and SHG, SHG from $MnBi_2Te_4$ compared to WSe_2, effect of surface oxidation on SHG, and laser-induced heating RMCD (PDF)

■ AUTHOR INFORMATION

Corresponding Author

Xiaodong Xu — *Department of Physics, University of Washington, Seattle, Washington 98195, United States; Department of Materials Science and Engineering, University of Washington, Seattle, Washington 98195, United States;* orcid.org/0000-0003-0348-2095; Email: xuxd@uw.edu

Authors

Jordan Fonseca — *Department of Physics, University of Washington, Seattle, Washington 98195, United States;* orcid.org/0000-0002-6325-3246

Geoffrey M. Diederich — *Department of Physics, University of Washington, Seattle, Washington 98195, United States; Intelligence Community Postdoctoral Research Fellowship Program, University of Washington, Seattle, Washington 98195, United States*

Dmitry Ovchinnikov — *Department of Physics, University of Washington, Seattle, Washington 98195, United States;* orcid.org/0000-0002-8971-1639

Jiaqi Cai — *Department of Physics, University of Washington, Seattle, Washington 98195, United States;* orcid.org/0000-0002-7829-9554

Chong Wang — *Department of Materials Science and Engineering, University of Washington, Seattle, Washington 98195, United States*

Jiaqiang Yan — *Materials Science and Technology Division, Oak Ridge National Laboratory, Oak Ridge, Tennessee 37831, United States; Department of Materials Science and Engineering, University of Tennessee, Knoxville, Tennessee 37996, United States*

Di Xiao — *Department of Physics, University of Washington, Seattle, Washington 98195, United States; Department of Materials Science and Engineering, University of Washington, Seattle, Washington 98195, United States*

Complete contact information is available at: https://pubs.acs.org/10.1021/acs.nanolett.2c04010

Author Contributions

X.X conceived the experiment. J.F. prepared samples, assisted by D.O. and J.C. G.M.D. and J.F. performed the RMCD and SHG measurements. C.W. and D.X. verified the SHG theoretical calculations. J.Y. synthesized and characterized the bulk crystals. J.F., G.M.D., D.O., and X.X. analyzed the data and wrote the paper, with input from all authors. All authors discussed the results. J.F. and G.M.D. contributed equally to this work.

Notes

The authors declare no competing financial interest.

■ ACKNOWLEDGMENTS

We thank Kyle Seyler for helpful discussion during the preparation of this manuscript. This work was mainly supported by the Department of Energy, Basic Energy Sciences, Materials Sciences and Engineering Division (DE-SC0012509). Magneto-optical measurement is partially supported as part of Programmable Quantum Materials, an Energy Frontier Research Center funded by the U.S. Department of Energy (DOE), Office of Science, Basic Energy Sciences (BES), under award DE-SC0019443. Device fabrication is partially supported by AFOSR FA9550-21-1-0460. J.Y. acknowledges support from the U.S. Department of Energy, Office of Science, Basic Energy Sciences, Materials Sciences and Engineering Division. The authors also acknowledge the use of the facilities and instrumentation supported by NSF MRSEC DMR-1719797. This research was supported by an appointment to the Intelligence Community Postdoctoral Research Fellowship Program at the University of Washington, administered by Oak Ridge Institute for Science and Education through an interagency agreement between the U.S. Department of Energy and the Office of the Director of National Intelligence. X.X. acknowledges the support from the State of Washington funded Clean Energy Institute.

■ REFERENCES

(1) Otrokov, M. M.; et al. Prediction and observation of an antiferromagnetic topological insulator. *Nature* **2019**, *576*, 416−422.

(2) Liu, C.; et al. Robust axion insulator and Chern insulator phases in a two-dimensional antiferromagnetic topological insulator. *Nat. Mater.* **2020**, *19*, 522−527.

(3) Ge, J.; et al. High-Chern-number and high-temperature quantum Hall effect without Landau levels. *Natl. Sci. Rev.* **2020**, *7*, 1280−1287.

(4) Ovchinnikov, D.; et al. Intertwined Topological and Magnetic Orders in Atomically Thin Chern Insulator MnBi2Te4. *Nano Lett.* **2021**, *21*, 2544−2550.

(5) Gao, A.; et al. Layer Hall effect in a 2D topological axion antiferromagnet. *Nature* **2021**, *595*, 521−525.

(6) Deng, Y.; et al. Quantum anomalous Hall effect in intrinsic magnetic topological insulator MnBi2Te4. *Science* **2020**, *367*, 895−900.

(7) Yang, S.; et al. Odd-Even Layer-Number Effect and Layer-Dependent Magnetic Phase Diagrams in MnBi2Te4. *Phys. Rev. X* **2021**, *11*, 011003.

(8) Yan, J.-Q.; et al. Crystal growth and magnetic structure of MnBi2Te4. *Phys. Rev. Mater.* **2019**, 3, 064202.

(9) Otrokov, M. M.; et al. Prediction and observation of an antiferromagnetic topological insulator. *Nature* **2019**, *576*, 416−422.

(10) Otrokov, M. M.; et al. Unique Thickness-Dependent Properties of the van der Waals Interlayer Antiferromagnet MnBi2Te4 Films. *Phys. Rev. Lett.* **2019**, *122*, 107202.
(11) Liu, C.; et al. Robust axion insulator and Chern insulator phases in a two-dimensional antiferromagnetic topological insulator. *Nat. Mater.* **2020**, *19*, 522−527.
(12) Ying, Z.; et al. Experimental evidence for dissipationless transport of the chiral edge state of the high-field Chern insulator in MnBi2Te4 nanodevices. *Phys. Rev. B* **2022**, *105*, 85412.
(13) Hu, C.; et al. Growth, characterization, and Chern insulator state in MnBi2Te4 via the chemical vapor transport method. *Phys. Rev. Mater.* **2021**, *5*, 124206.
(14) Li, Y.; et al.Nonlocal Transport and One-dimensional Conduction in the Axion Insulator State of $MnBi_2Te_4$. *arXiv*2022; DOI: 10.48550/arXiv.2105.10390 (accessed September 13, 2022).
(15) Cai, J.; et al. Electric control of a canted-antiferromagnetic Chern insulator. *Nat. Commun.* **2022**, *13*, 1668.
(16) Liu, C.; et al. Magnetic-field-induced robust zero Hall plateau state in MnBi2Te4 Chern insulator. *Nat. Commun.* **2021**, *12*, 4647.
(17) Gao, A.; et al. Layer Hall effect in a 2D topological axion antiferromagnet. *Nature* **2021**, *595*, 521−525.
(18) Shikin, A. M.; et al. Nature of the Dirac gap modulation and surface magnetic interaction in axion antiferromagnetic topological insulator MnBi2Te4. *Sci. Rep* **2020**, *10*, 15.
(19) Chen, Y. J.; et al. Topological Electronic Structure and Its Temperature Evolution in Antiferromagnetic Topological Insulator MnBi2Te4. *Phys. Rev. X* **2019**, *9*, 041040.
(20) Hao, Y. J.; et al. Gapless Surface Dirac Cone in Antiferromagnetic Topological Insulator MnBi2Te4. *Phys. Rev. X* **2019**, *9*, 041038.
(21) Yan, J.-Q. Perspective−The Elusive Quantum Anomalous Hall Effect in MnBi2Te4: Materials. *ECS Journal of Solid State Science and Technology* **2022**, *11*, 063007.
(22) Hou, F.; et al. Te-Vacancy-Induced Surface Collapse and Reconstruction in Antiferromagnetic Topological Insulator MnBi2Te4. *ACS Nano* **2020**, *14*, 11262−11272.
(23) Lin, Z.; et al. Magnetism and Its Structural Coupling Effects in 2D Ising Ferromagnetic Insulator VI3. *Nano Lett.* **2021**, *21*, 9180−9186.
(24) Li, T.; et al. Pressure-controlled interlayer magnetism in atomically thin CrI3. *Nat. Mater.* **2019**, *18*, 1303−1308.
(25) Song, T.; et al. Switching 2D magnetic states via pressure tuning of layer stacking. *Nat. Mater.* **2019**, *18*, 1298−1302.
(26) Li, Y.; et al. Probing symmetry properties of few-layer MoS2 and h-BN by optical second-harmonic generation. *Nano Lett.* **2013**, *13*, 3329−3333.
(27) Malard, L. M.; Alencar, T. v.; Barboza, A. P. M.; Mak, K. F.; de Paula, A. M. Observation of intense second harmonic generation from MoS2 atomic crystals. *Phys. Rev. B* **2013**, *87*, 201401.
(28) Mennel, L.; et al. Second harmonic generation in strained transition metal dichalcogenide monolayers: MoS2, MoSe2, WS2, and WSe2. *APL Photonics* **2019**, *4*, 034404.
(29) Yang, F.; et al. Tunable Second Harmonic Generation in Twisted Bilayer Graphene. *Matter* **2020**, *3*, 1361−1376.
(30) Yao, K.; et al. Enhanced tunable second harmonic generation from twistable interfaces and vertical superlattices in boron nitride homostructures. *Sci. Adv.* **2021**, *7*, No. eabe8691.
(31) Hsu, W. T.; et al. Second harmonic generation from artificially stacked transition metal dichalcogenide twisted bilayers. *ACS Nano* **2014**, *8*, 2951−2958.
(32) Schaibley, J. R.; et al. Directional interlayer spin-valley transfer in two-dimensional heterostructures. *Nat. Commun.* **2016**, *7*, 13747.
(33) Fiebig, M.; et al. Second harmonic generation and magnetic-dipole-electric-dipole interference in antiferromagnetic Cr2O3. *Phys. Rev. Lett.* **1994**, *73*, 2127−2130.
(34) Chu, H.; et al. Linear Magnetoelectric Phase in Ultrathin MnPS3 Probed by Optical Second Harmonic Generation. *Phys. Rev. Lett.* **2020**, *124*, 027601.
(35) Sun, Z.; et al. Giant nonreciprocal second-harmonic generation from antiferromagnetic bilayer CrI3. *Nature* **2019**, *572*, 497−501.
(36) Ni, Z.; et al. Imaging the Néel vector switching in the monolayer antiferromagnet MnPSe3 with strain-controlled Ising order. *Nat. Nanotechnol* **2021**, *16*, 782−787.
(37) Li, H.; et al. Antiferromagnetic topological insulator MnBi2Te4: Synthesis and magnetic properties. *Phys. Chem. Chem. Phys.* **2020**, *22*, 556−563.
(38) Yan, J. Q.; et al. Evolution of structural, magnetic, and transport properties in MnBi2-xSbxTe4. *Phys. Rev. B* **2019**, *100*, 104409.
(39) Pei, C.-Y.; et al. Pressure-Induced Topological and Structural Phase Transitions in an Antiferromagnetic Topological Insulator. *Chin. Phys. Lett.* **2020**, *37*, 066401.
(40) Ding, L.; et al. Crystal and magnetic structures of magnetic topological insulators MnBi2Te4 and MnBi4Te7. *Phys. Rev. B* **2020**, *101*, 020412.
(41) Fei, R.; et al. Giant photogalvanic effect and second-harmonic generation in magnetic axion insulators. *Phys. Rev. B* **2020**, *102*, 35440.
(42) Huang, B.; et al. Layer-dependent ferromagnetism in a van der Waals crystal down to the monolayer limit. *Nature* **2017**, *546*, 270−273.
(43) Hsieh, D.; et al. Nonlinear optical probe of tunable surface electrons on a topological insulator. *Phys. Rev. Lett.* **2011**, *106*, 057401.
(44) Li, J.; et al. Intrinsic magnetic topological insulators in van der Waals layered MnBi2Te4-family materials. *Sci. Adv.* **2019**, *5*, 6.
(45) Lee, K.; et al. Magnetic Order and Symmetry in the 2D Semiconductor CrSBr. *Nano Lett.* **2021**, *21*, 3511−3517.
(46) McIver, J. W.; et al. Theoretical and experimental study of second harmonic generation from the surface of the topological insulator Bi2Se3. *Phys. Rev. B* **2012**, *86*, 35327.

https://doi.org/10.1021/acs.nanolett.2c04010
Nano Lett. 2022, 22, 10134−10139